

26. T. S. Arrhenius *et al.*, *Proc. Natl. Acad. Sci. U.S.A.* **83**, 5355 (1986).
27. The authors thank H. B. Gray and H. H. Thorp for useful discussions and acknowledge the Office of Naval Research (contract N00014-K-0377), the Department of Energy's Energy Conversion and Utilization Technologies Division for support of the work performed at the Jet Propulsion Laboratory,

California Institute of Technology through an agreement with the National Aeronautics and Space Administration, and the Brazilian agencies CNPq and FINEP for support of this work. The work was performed, in part, during a visit by J.N.O. to the Jet Propulsion Laboratory.

25 March 1988; accepted 13 June 1988

Simulation of Eolian Saltation

ROBERT S. ANDERSON* AND PETER K. HAFF

Saltation is important in the transport of sand-sized granular material by wind and in the ejection of dust from the bed both on Earth and on Mars. The evolution of the saltating population and all its characteristic profiles is calculated from inception by pure aerodynamic entrainment through to steady state. Results of numerical simulations of single-grain impacts into granular beds are condensed into analytic expressions for the number and speeds of grains rebounding or ejected (splashed) from the bed. A model is combined with (i) this numerical representation, (ii) an expression for the aerodynamic entrainment rate, and (iii) the modification of the wind velocity profile by saltating grains. Calculated steady state mass fluxes are within the range of mass fluxes measured in wind tunnel experiments; mass flux is nonlinearly dependent on the shear velocity. Aerodynamically entrained grains in the system are primarily seeding agents; at steady state, aerodynamic entrainment is rare. The time for the entire system to reach steady state is roughly 1 second, or several long-trajectory hop times.

SALTATION IS THE PRIMARY MEANS BY which sand-sized particles travel in most realistic winds (1). In pure saltation, particles travel smooth paths that are essentially unaffected by turbulent fluctuations of the wind between periodic encounters with the bed; as grain size decreases or wind velocity increases, saltation grades into pure suspension (2, 3), where turbulent fluctuations dominate the trajectories. Understanding the physics of blown sand is necessary for accurate prediction of sediment transport on Mars (4) and soil loss due to wind erosion (5), for understanding the origin of such geomorphic features as ventifacts (6) and ripples (7, 8), and for reconstruction of environmental conditions from the eolian rock record (9, 10). Wind tunnel saltation experiments (4, 11, 12) have led to empirical relations between the total mass flux and a characteristic wind velocity, typically chosen to be the shear velocity, u_* (13). Profiles of mass flux, $q_m(z)$, and concentration, $c(z)$, decay monotonically and sharply above the bed both in blowing snow (14) and in blowing sand (4, 11, 12). In addition, natural obstacles have erosion profiles that indicate a distinct maximum in abrasion above the bed (15, 16); such profiles con-

strain the pattern of kinetic-energy flux to the obstacle (6).

Earlier workers (1, 3, 17, 18) recognized that the initial launch velocities (speed and angle) of grains ejected from the bed are diverse. They used the various profile data to constrain the probability distribution of these velocities. Grain trajectories were integrated forward in time and mass flux and concentration were calculated as each trajectory passed first upward, then downward through a particular height element. Each trajectory and the resulting mass flux and concentration profiles were then weighted according to a chosen probability distribution, the parameters of which were altered

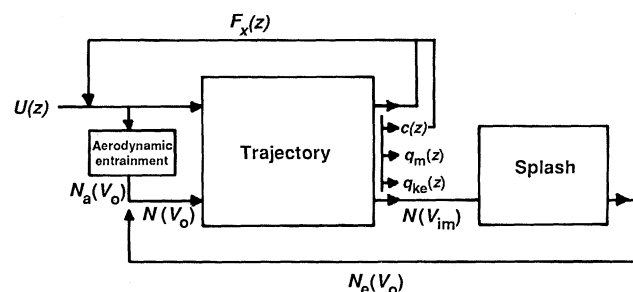
until a match was achieved with an appropriate empirically derived profile. Importantly, these matches required a knowledge of the total number of grains in saltation. Typically, the total calculated mass flux was forced to obey an empirically derived relation to the shear velocity (that is, the mass-flux "law") (3). In these models the preponderance of grains travel in low-speed, near-bed trajectories; the highest liftoff speeds are the least likely, as observed in nature.

Although the models calibrated for mass flux yielded reasonable concentration and kinetic-energy flux profiles (6), they had several severe deficiencies. Reliance on a mass-flux law to set the total number of grains in saltation precluded insight into how the mass flux and the probability distribution of the initial velocities emerged from the physics of the problem. The models were also unable to provide information about the shape of the wind velocity profile. In addition, because nothing was learned about the time scales involved in the approach to steady state saltation (the calibrations were with steady state wind tunnel data), no foundation was laid for the treatment of the more complex case of a variable wind.

Many of the deficiencies of these models can be removed by incorporating the physics of (i) the grain-bed interaction and (ii) the feedback involved in the extraction of momentum from the wind by the accelerating grains (Fig. 1). The grain-bed interaction sets the probability distribution of the initial conditions, and the wind velocity alteration is responsible for eventually limiting the total number of grains in transport. (The energy in the wind is the limiting resource available for the growth of the saltation population.)

We performed numerical simulations of single-grain impacts into a granular bed to evaluate quantitatively the splash process.

Fig. 1. Schematic diagram of the processes involved in the eolian saltation system. Initial wind velocity profile, $U(z)$, sets aerodynamic entrainment rate, $N_a(V_0)$, in grains per unit area per unit time being ejected from the bed with the lowest possible velocity (V_{0mp}). Grain trajectories are calculated, resulting in profiles of concentration, $c(z)$, mass flux, $q_m(z)$, kinetic energy flux, $q_{ke}(z)$, and horizontal force on the wind, $F_x(z)$, as well as the impact velocities of each grain trajectory, V_{im} . The grain splash is calculated for each impact according to a probabilistic description (26), resulting in a new number of ejecta, $N_c(V_0)$ (including both rebounding and splashed grains), in each of the initial velocity "bins." At each time step the wind velocity profile is modified according to the imposed force profile, resulting in a new shear stress at the bed and a corresponding change in the aerodynamic entrainment rate. The new splash ejecta are added to the new aerodynamically entrained grains to produce the total number of grains leaving the bed at the next step, $N(V_0)$, and the calculation is repeated until a steady state is achieved.



Division of Physics, Mathematics and Astronomy, California Institute of Technology, Pasadena, CA 91125.

*Present address: Earth Sciences Board, University of California, Santa Cruz, CA 95064.

The impact simulations were performed in two dimensions with identical, slightly inelastic, 1-mm-diameter grains (disks). Interactions between grains were characterized by a coefficient of restitution, an intergrain friction coefficient, and an elastic modulus (19). We generated beds by dropping 87 particles with random initial velocities into a box with periodic boundaries (wraparound conditions that force what goes off one side of the calculation space to reenter on the other), its width chosen such that the resulting bed was about ten grains deep. Three such granular beds with different packing configurations were each impacted 20 times to develop the splash statistics for each impact angle and speed. These computations are more realistic than earlier numerical work on impact dynamics (20) in which the bed was assumed to be hexagonally packed; such beds greatly restrict the range of possible ejection angles.

The results of the grain splash numerical simulations are qualitatively similar to but more comprehensive than those derived from earlier numerical (20) and physical experiments (21–23), especially for low-speed impacts (Fig. 2). In our simulations the impacting grains rebounded from the surface with nearly unit (0.95) probability, a result postulated by Kobayashi (14) and Rumpel (24). For the chosen grain parameters (19), the mean rebound speed is approximately 50 to 60% of the impact speed (Fig. 2C), and the mean rebound angle is 30° to 40° from the horizontal (Fig. 2D). An impact also ejects a number of grains from within a few grain diameters of the impact site. The mean number of grains ejected increases roughly linearly with impact speed; this relation compares well with data

obtained from physical impact experiments with coarse sand (22, 23) (Fig. 2B). The mean speed of the ejected particles appears to saturate at ~10% of the speed of the impacting grain (Fig. 2C), and the mean ejection angle tends to be oriented downwind at 60° to 70° from the horizontal (Fig. 2D). All of these results are only slightly dependent on the impact angle for impacts between 8° and 15°, which cover the range

of expected impact angles in eolian saltation (1, 3, 13). The results are expressed in terms of the splash function (25), an analytic expression for the number density of grains ejected from the bed and their distribution of initial velocities for a given impact velocity (26).

Aerodynamic forces of lift and drag may also entrain grains directly. Aerodynamic entrainment is required for the initiation of saltation in the absence of external mechanical disturbances. As a simple model for aerodynamic entrainment, we take the number of entrained grains per unit area per unit time, N_a , to be proportional to the excess shear stress

$$N_a = \alpha(\tau_a - \tau_c) \quad (1)$$

where τ_a is the short-term mean shear stress at the bed, τ_c is the critical fluid shear stress for entrainment, for which an expression has been determined from numerous wind tunnel experiments (4, 13, 27), and α is a constant. We assumed that all such aerodynamically entrained grains leave the bed with the lowest possible velocity, that needed to reach a height of about one grain diameter, D , above the bed. This is a conservative assumption that limits the role of the aerodynamic grains in the eolian saltation process.

As grains are accelerated by the force of the wind, they impose an equal and opposite force on the wind. The profile of this force per unit volume on the wind was calculated (18, 24, 28) and used to alter the effective stress available to shear the air at all levels in the flow.

Inputs required for the full simulation of the eolian saltation system are (i) an initial wind velocity (U) profile, taken to be logarithmic

$$U = (u_* / k) \ln(z/z_0) \quad (2)$$

where k is von Karman's constant ($= 0.4$), and z_0 is the initial effective roughness of the bed related to the size and packing of the stationary sand grains in the bed ($= D/30$). The shear velocity, u_* , in turn sets the initial shear stress at the bed [$(\tau_a)_0 = \tau_b = \rho_a u_*^2$, where ρ_a is the density of air]; (ii) the splash function derived from the numerical simulations described above; and (iii) the coefficient of proportionality between the excess shear stress and the aerodynamic entrainment rate.

In the simulated evolution of the saltation population (Figs. 3 and 4), initial entrainment is entirely aerodynamic. These grains gain horizontal momentum from the wind and impact with velocities such that a small proportion rebound with greater initial velocities than those of the initial trajectories; few subsequent grains are splashed at this

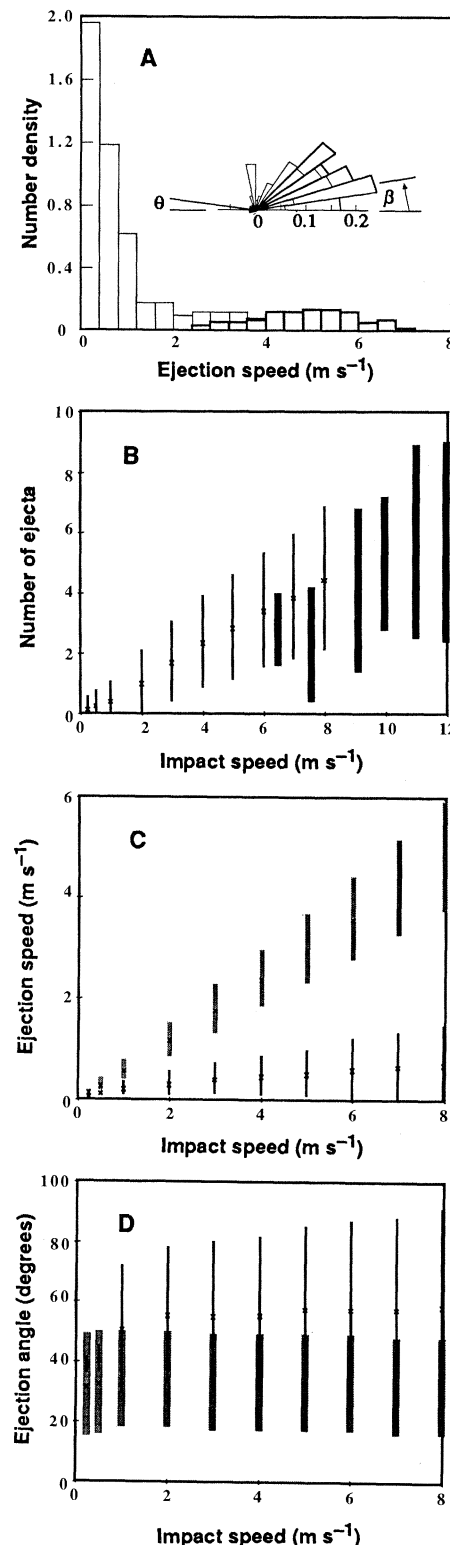


Fig. 2. Results of numerical simulations of grain impacts, for impact angle, θ , of 8°, $D = 1$ mm. (A) Histogram showing number of ejecta in each of several ejection speed bins, expected from a single impact with a speed of 8 m s⁻¹, showing contributions from both splashed (light lines) and rebounding (heavy lines) populations. Statistics assembled from a total of 60 impact events, 20 on each of three distinct beds. Note normal distribution of rebound speeds and exponential distribution of splash speeds, with means as shown in (C). Rose diagram (inset) depicts the probability density of the ejection angle, β , in 10° bins for rebounds (heavy lines) and splashed grains (light lines). Although widely spread, the mean rebound angle is typically greater than the impact angle, whereas the splashed grains are ejected at even higher angles [see (C)]. (B) Number of grains splashed from the bed for each of ten impact speed cases (cross = mean, bar = 1 σ on either side of the mean). Also shown (bold bars) are data from coarse sand ($D = 0.8$ mm) impact experiments (22, 23) (bars are half-widths on either side of the mean). (C) Ejection speed and (D) ejection angle for rebounding (patterned) and splashed (clear) grains as functions of impact speed.

stage. An initial delta function probability distribution of liftoff velocities therefore evolves to a broader probability distribution, filling out to the higher velocities. The grains with higher liftoff velocities are air-

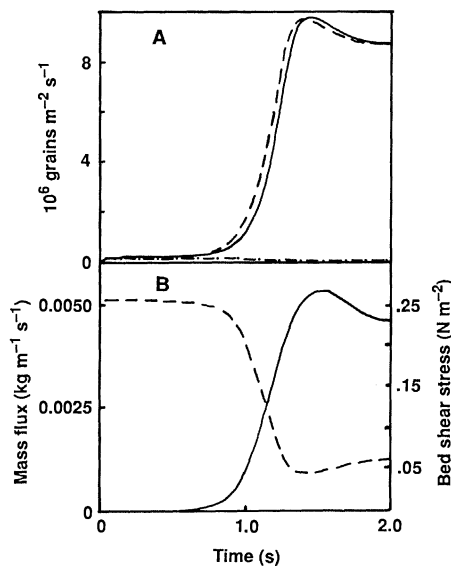


Fig. 3. Simulation of saltation system for $u_* = 0.5 \text{ m s}^{-1}$, $D = 0.25 \text{ mm}$. (A) Numbers of grains impacting (dashed), being ejected (rebound plus splash, solid), and being entrained aerodynamically (dot-dashed) as functions of time, and (B) corresponding histories of total mass flux (solid) and shear stress at the bed (dashed).

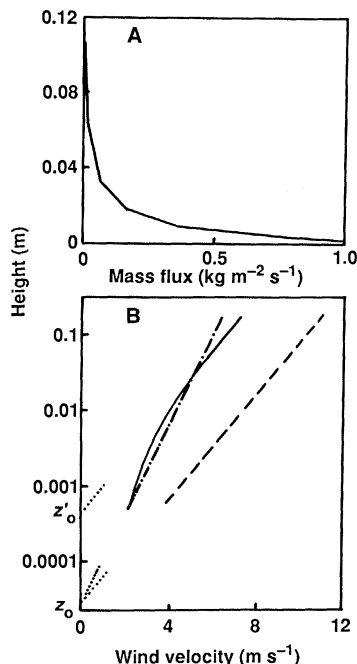


Fig. 4. Steady state (A) mass-flux profile and (B) wind velocity profile (solid line). Note logarithmic height scale in (B). Also shown in (B) are the initial wind velocity profile (dashed); threshold wind velocity profile (dot-dashed) associated with the roughness height, z_0 (dotted lines indicate extrapolation to $U = 0$ intercept); and the final effective roughness, z_0' .

borne for longer periods of time before impacting and contribute more strongly to the splash ejection of other grains. The full range of possible ejection velocities is populated only after many tens of small trajectory times. At this point the total number of grains in transport begins to grow rapidly, the highest impact velocity grains being most efficient in splashing grains into the airstream. The resulting, roughly exponential growth of the number of grains in saltation is curtailed only when the extraction of momentum from the wind is sufficient to alter significantly the wind velocity profile, which in turn alters the impact velocities of the grains with long trajectories.

The system eventually reaches a steady state characterized by a specific total mass flux, an equal number of impacting and ejected grains, and a stationary wind velocity profile. The overshoot of the steady state (Fig. 3) appears to be due to the time lag associated with the 0.2- to 0.3-s hop times of the most energetic trajectories responsible for the majority of the ejections from the bed. The steady state mass flux is well within the range of fluxes measured in wind tunnel studies for the same combination of shear velocity and grain size (13). Whereas the initial saltation population is entirely aerodynamic, the steady state saltation population for most imposed shear velocities contains no aerodynamically entrained grains. As the population of splashed and rebounding grains increases, the shear stress at the bed is reduced, which produces a corresponding decrease in the rate of aerodynamic entrainment. The steady state shear stress at the bed is reduced to slightly below the critical shear stress for aerodynamic entrainment. The effective roughness of the bed is simultaneously greatly increased, as reflected in the rise of the $U = 0$ intercept (from z_0 to z_0' in Fig. 4). This change in bed roughness is in accord with numerous measured wind velocity profiles during saltation experiments, as summarized by Owen (29). Also, the resulting steady state profile of mass flux (Fig. 4) decreases rapidly above the bed, implying that the system has evolved to produce a realistic probability distribution for the initial trajectory velocities (30). By varying the initial shear velocity, we produced a mass flux relation that is broadly similar to those derived empirically: above a threshold shear velocity [$u_{*c} = (\tau_c/\rho_a)^{1/2}$], the flux increases as a power of $(u_* - u_{*c})$ (Fig. 5).

The response time of the saltation system appears to be approximately 1 to 2 s, or several long trajectory times (31). For the cases run, it appears that the response time is a weak function of the shear velocity. It is

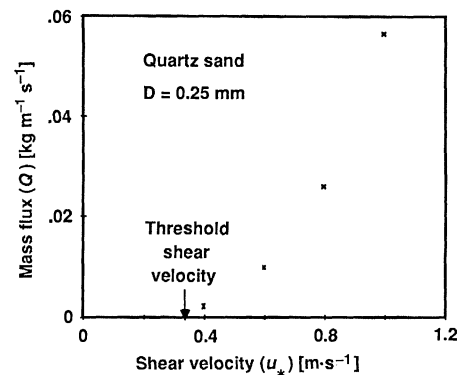


Fig. 5. Total mass flux as a function of shear velocity: a calculated mass-flux "law" for grains of diameter 0.25 mm, density 2650 kg m^{-3} . Note the nonlinear dependence of the flux on the excess shear velocity, $(u_* - u_{*c})$, where u_{*c} is the critical shear velocity needed to entrain grains aerodynamically.

long for low shear velocities. A knowledge of the response time, which is difficult to obtain from wind tunnel experiments, will allow us to treat the problem of predicting total mass fluxes in variable winds.

This model can be extended to saltation of snow by changing the elastic properties and the density of the grains, and to more exotic systems such as saltation in the martian environment by changing the characteristics of the atmosphere. To extend the model to the multiple-grain size system the granular splash must be modified to incorporate beds composed of grains of several diameters. Accounts must be kept for the number and speeds of grains of each grain size class ejected from the bed by the impact of a grain from any other class. Studies of this kind will be especially important in establishing the link between saltation and the ejection of fines (that is, dust) into the atmosphere, where the fines will travel in suspension. Ejection of fines into suspension is known to occur simultaneously with the initiation of saltation in mixed-grain size systems (5), presumably because of impact lofting of smaller particle sizes that are not entrained easily by direct fluid forces.

REFERENCES AND NOTES

1. R. A. Bagnold, *The Physics of Blown Sand and Desert Dunes* (Methuen, London, 1941).
2. R. S. Anderson, *J. Geol.* **95**, 497 (1987).
3. ——— and B. Hallet, *Geol. Soc. Am. Bull.* **97**, 523 (1986).
4. R. Greeley et al., *J. Geophys. Res.* **87**, 10,009 (1982).
5. D. A. Gillette, *Geol. Soc. Am. Spec. Pap.* **186**, 11 (1981).
6. R. S. Anderson, *Geol. Soc. Am. Bull.* **97**, 1270 (1986).
7. J. M. Ellwood et al., *J. Sediment Pet.* **45**, 554 (1975).
8. R. S. Anderson, *Sedimentology* **34**, 943 (1987).
9. ———, *ibid.* **35**, 175 (1988).
10. R. A. Hunter, *ibid.* **32**, 409 (1985).
11. G. P. Williams, *ibid.* **9**, 89 (1964).
12. A. W. Zingg, *Univ. Iowa Studies Eng.* **24**, 111 (1953).

13. R. Greeley and J. D. Iversen, *Wind as a Geologic Process* (Cambridge Univ. Press, Cambridge, 1985).
14. D. Kobayashi, *Contrib. Inst. Low Temp. Studies* **A24**, 1 (1972).
15. R. P. Sharp, *Geol. Soc. Am. Bull.* **75**, 785 (1964).
16. ———, *ibid.* **91**, 724 (1980).
17. J. L. Jensen and M. Sorenson, *Sedimentology* **33**, 547 (1986).
18. M. Sorenson, in *International Workshop on the Physics of Blown Sand*, O. E. Barndoff-Nielson et al., Eds. (University of Aarhus, Aarhus, Denmark, 1986), vol. 1, pp. 141–190.
19. The motion of particles in the bed is followed by integrating numerically the equations of motion of each particle as it moves under the influence of gravity and grain-grain contact forces. Both normal and frictional forces act at each such contact, and particles may rotate in response to unbalanced torques. Because all grains in the system are followed, no artificial distinction is made between surface grains and grains below the surface. A value of 0.7 was used for the coefficient of restitution and value of 0.5 was used for the surface friction. Anecdotal numerical experiments have failed to reveal that the results are significantly dependent on these quantities (R. S. Anderson and P. K. Haff, in preparation).
20. B. T. Werner and P. K. Haff, in *Advances in Aerodynamics, Fluid Mechanics, and Hydraulics*, R. E. A. Arndt et al., Eds. (American Society of Civil Engineers, New York, 1986), pp. 337–345; B. T. Werner and P. K. Haff, *Sedimentology* **35**, 189 (1988).
21. S. Mitha et al., *Acta Mech.* **63**, 267 (1986).
22. B. B. Willetts and M. A. Rice, in *International Workshop on the Physics of Blown Sand*, O. E. Barndoff-Nielson et al., Eds. (University of Aarhus, Aarhus, Denmark, 1986), vol. 1, pp. 83–100.
23. B. T. Werner, thesis, California Institute of Technology (1987), for single-grain impact experiments with coarse sand.
24. D. A. Rumpel, *Sedimentology* **32**, 267 (1985).
25. J. E. Ungar and P. K. Haff, *ibid.* **34**, 289 (1987).
26. The number of grains ejected, $N_e(V_0)$, in each of several ejection-velocity bins of width dV_0 , because of a single impact of velocity V_{im} , may be expressed as the sum of the number due to rebound, $N_r(V_0)$, and the number due to splash, $N_s(V_0)$, where

$$N_r(V_0) = \alpha_r \{1/[\gamma_r V_{im} (2\pi)^{1/2}] \cdot \exp \{-[V_0 - (d_r V_{im})]^2 / [2(\gamma_r V_{im})^2]\} dV_0$$

a normal distribution with mean = $d_r V_{im}$ and standard deviation = $\gamma_r V_{im}$ and

$$N_s(V_0) = \alpha_s V_{im} [1/d_s V_{im}] \cdot \exp [-V_0/(d_s V_{im})] dV_0$$

an exponential distribution with mean and standard deviation = $d_s V_{im}$ (see Fig. 2A). The sum over all V_0 increments must be equal to the total number of

- grains rebounding and splashed from the event, taken to be α_r (a constant) for the rebounds, and ($\alpha_s V_{im}$) for the splashed grains. Our results suggest that $\alpha_r = 0.95$, $d_r = 0.59$, $\gamma_r = 0.12$, $\alpha_s = 0.6 \text{ sm}^{-1}$, and $d_s = 0.1$.
27. J. D. Iversen, et al., *Icarus* **29**, 381 (1976).
28. R. S. Anderson, thesis, University of Washington (1986).
29. P. R. Owen, *J. Fluid. Mech.* **20**, 225 (1964).
30. A close analogy may be drawn between the saltation population ultimately limited to its steady state value by the energy available in the wind, and a biological population limited to its carrying capacity by a fixed resource base. In this analogy the probability distribution of trajectories corresponds roughly to the age structure of the biological population.
31. The response time diminishes by only 20% for a tenfold increase in α , the proportionality constant in Eq. 1, illustrating the dominant role played by the trajectory times of the high-energy trajectories (0.2 to 0.3 s) in establishing the response time.
32. We thank B. T. Werner and S. Spickelmire for sharing their insights into this problem. We also acknowledge the helpful suggestions of three anonymous reviewers. This work was supported by the U.S. Army Research Office, contract DAAL-03-86-K-0132.

12 April 1988, accepted 10 June 1988

Relaxation of Isolated Ventricular Cardiomyocytes by a Voltage-Dependent Process

JOHN H. B. BRIDGE, KENNETH W. SPITZER, PHILIP R. ERSHLER

Cell contraction and relaxation were measured in single voltage-clamped guinea pig cardiomyocytes to investigate the contribution of sarcolemmal Na^+ - Ca^{2+} exchange to mechanical relaxation. Cells clamped from -80 to 0 millivolts displayed initial phasic and subsequent tonic contractions; caffeine reduced or abolished the phasic and enlarged the tonic contraction. The rate of relaxation from tonic contractions was steeply voltage-dependent and was significantly slowed in the absence of a sarcolemmal Na^+ gradient. Tonic contractions elicited in the absence of a Na^+ gradient promptly relaxed when external Na^+ was applied, reflecting activation of Na^+ - Ca^{2+} exchange. It appears that a voltage-dependent Na^+ - Ca^{2+} exchange can rapidly mechanically relax mammalian heart muscle.

ALTHOUGH UNIMPAIRED RELAXATION is essential for normal heart function, the mechanism of relaxation in mammalian ventricular muscle is not fully understood. Relaxation continues even in the presence of caffeine. However, there is evidence that the sarcoplasmic reticulum (SR) becomes significantly more permeable to Ca^{2+} so that it cannot sequester this ion (1–3). Under these conditions the decline in cytosolic calcium required for relaxation may be mediated by sarcolemmal Na^+ - Ca^{2+} exchange (4). Moreover, this relaxation should be voltage-sensitive if the exchange is voltage-sensitive. In fact, mechanical relaxation in amphibian heart, which is thought to be dependent on Na^+ -

Ca^{2+} exchange, displays both Na^+ (5) and voltage dependence (6). In this study we examined the contribution of Na^+ - Ca^{2+} exchange to the relaxation of voltage-clamped guinea pig ventricular myocytes.

Myocytes were isolated by perfusion of guinea pig hearts with a nominally Ca^{2+} -

free bicarbonate-buffered solution containing collagenase (1 mg/ml) and hyaluronidase (1 mg/ml). Cells were dispersed in a modified Tyrode's solution containing 50 μM Ca^{2+} , which was subsequently brought to 1.0 mM for cell storage. Normal Tyrode's solution contained (in millimoles per liter): 126.0 NaCl, 4.4 KCl, 5.0 MgCl_2 , 18.0 NaHCO_3 , 2.7 CaCl_2 , 0.33 NaH_2PO_4 , and 11.0 dextrose and was gassed with 5% CO_2 and 95% O_2 . Sodium-free solution contained (in millimoles per liter): 138.0 LiCl, 4.4 KCl, 5.0 MgCl_2 , 2.7 CaCl_2 , Hepes 12.0, LiOH 6.4, and 11.0 dextrose. Its control solution had the same composition except that NaCl and NaOH replaced LiCl and LiOH, respectively. Hepes-buffered solutions were gassed with 100% O_2 . The pH of all solutions was 7.4. Cells rested on the glass bottom of a tissue bath and were continuously bathed with Tyrode's solutions at $30^\circ \pm 0.2^\circ\text{C}$. Complete replacement of the bath solution required ≤ 2 seconds.

Single cells were voltage-clamped at a

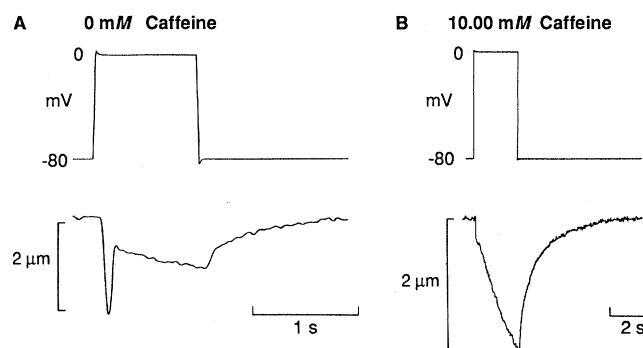


Fig. 1. Cell contraction (measured as shortening) in the absence and presence of 10.0 mM caffeine. (A) The cell was voltage-clamped from -80 to 0 mV for 1 second. (B) Another cell was exposed to 10.0 mM caffeine and subjected to a 2-second clamp of the same magnitude.

Nora Eccles Harrison Cardiovascular Research and Training Institute and the Department of Medicine, University of Utah, Salt Lake City, UT 84112.